A Ray-Tracing Method for Modeling Indoor Wave Propagation and Penetration

Chang-Fa Yang, *Member IEEE,* Boau-Cheng Wu, and Chuen-Jyi Ko

***Abstract*—In this paper, a ray-tracing method for waves propagating inside building structures is presented. Ray tubes are used to model the wave propagation and penetration and all the significantly reflected and transmitted ray tubes from interfaces are included. Also, the cross sections of the ray tubes at the field points are evaluated to find the spreading factors of the waves and then the geometrical optics (GO) contributions at the locations of the receiving antenna. A program has been developed according to this ray-tracing technique that can be applied to simulate waves transmitted through and reflected from electrically large complex two-dimensional (2-D) and three-dimensional (3-D) bodies. To verify this ray-tracing program, 2-D moment method (MM) solutions for wave propagating in a two-room structure and also through a stair-shaped wall above a lossy ground are used to compare with those obtained from the ray tracing. Besides, comparisons of field measurements and ray-tracing simulations at 900 and 1800 MHz performed in a corridor on different floors and inside a staircase are shown. The effective complex dielectric constants of the building structures determined from a free-space method are employed in the simulations and a vector network analyzer is used for the field measurements. Good agreements are obtained. In addition, measured results for waves penetrating an exterior wall with metal-framed windows at 1290 MHz are employed to test the ray-tracing solutions, which indicate that scattering from the metal frames may be significant for field points near the windows. This ray-tracing program can be applied to evaluate the channel characteristics for the indoor wireless communications.**

***Index Terms*— Geometrical optics, indoor radio communication, ray-tracing method.**

I. Introduction

THIS paper presents a ray-tracing method for simulating indoor radio wave propagation and penetration. Similar problems had been studied by other investigators [1]–[7]. Total path loss per transmission of slab structures and multiple reflections from boundaries were included in their ray-tracing techniques to determine the geometrical optics (GO) contributions. In our method, those GO rays are traced by including multiple reflections and transmissions not only in the buildings, but also inside the material structures. The waves from a transmitting antenna are simulated by shooting many ray tubes, each composed of four rays, in all directions based on the far-field pattern of the antenna, and the spreading factors of the GO fields are evaluated from the cross-section area of the ray tubes. Wave propagation and penetration in electrically large two-dimensional (2-D) and three-dimensional (3-D) arbitrary bodies may be determined by applying this ray-tracing approach.

A 2-D moment method (MM) [8] is employed to compare with the ray-tracing method for 2-D lossy structures where both flat and stair-shaped slabs above a lossy ground are examined. The MM can provide numerically exact solutions, but is limited by the available memories and CPU time of the computer resources. However, by choosing the objects as small as just a few wavelengths, accurate MM results can be obtained to verify the ray-tracing program. For the 3-D problems, field measurements in a corridor on different floors and inside a staircase of the NTUST's buildings are performed and the results at 900 and 1800 MHz are compared with those obtained from the ray tracing. A vector-network analyzer, an amplifier, and two dipole antennas were used in those measurements. Open-site measurements with the two antennas separated 1 m apart and located 1.3 m above the ground were used as the reference for the indoor measurements. On the other hand, a 3-D ray-tracing program was developed to model the radio-wave propagation and penetration in buildings. The building structures are modeled as lossy dielectric blocks with uniform complex dielectric properties measured by using a free-space approach [9]. Comparisons of the measured and simulated results are shown; besides, measured data reported in [10] for waves at 1290 MHz coming through an external wall with metal-framed windows from a far distance are taken to examine the ray-tracing simulations.

The ray-tracing method is described in Section II. Section III presents the comparisons of the 2-D MM and the ray-tracing solutions. The field measurements and ray-tracing simulations for indoor wave propagation and penetration are discussed in Section IV. Conclusions are given in Section V.

II. Ray-Tracing Method

The waves from a transmitting antenna can be modeled as many ray tubes shooting from the location of the antenna [11]. In our ray-tracing program, every ray tube is composed of four rays defined by the increments of θ and ϕ ($\Delta\theta$ and $\Delta\phi$) in local spherical coordinates centered at the antenna, as shown in Fig. 1, and the ray tubes have about the same solid angle to improve program efficiency. To generate those ray tubes, a sphere of radius r centered at the antenna is divided into quadrilateral cells that are close to squares with approximately the same area by selecting a fixed $\Delta\theta$ and a $\Delta\phi$ about equal to $\Delta\theta/\sin\theta$. The value of θ at the center of each cell may be used

Manuscript received March 3, 1997; revised January 9, 1998. This work was supported by the R.O.C. National Science Council under Grants NSC 84-2221-E-011-001, NSC 85-2213-E-011-018, and NSC 86-2221-E-011-011.

The authors are with the Department of Electrical Engineering, National Taiwan University of Science and Technology, Taipei, Taiwan, R.O.C.

Publisher Item Identifier S 0018-926X(98)04620-1.

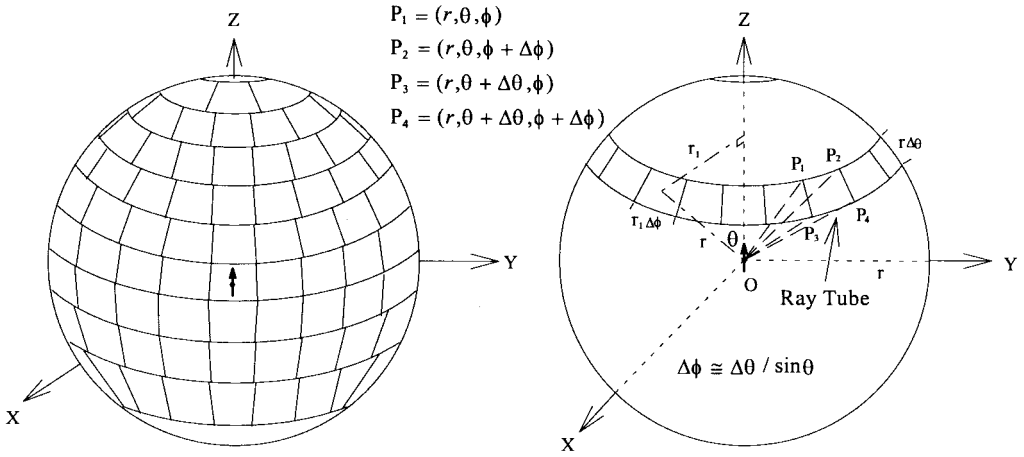

Fig. 1. Ray tubes are composed of four rays defined by $\Delta\theta$ and $\Delta\phi$ in the local spherical coordinates centered at the transmitting antenna and the solid angles of the tubes are about the same.

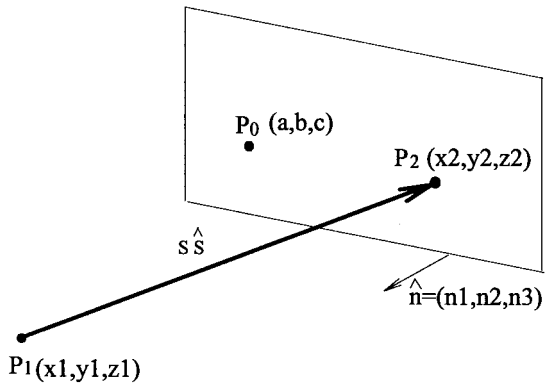

Fig. 2. A ray propagates from P_1 to P_2 on an intercepting plane.

to determine $\Delta\theta/\sin\theta$, which is then adjusted for $\Delta\phi$ to obtain an integer number of cells along the ϕ coordinate. Besides, for the dipole antenna, the axis of the dipole is chosen to be the local z axis of the spherical coordinates so that the field strengths of the initial tubes are symmetry in ϕ and the tubes along the local z axis can be neglected. Only the significant radiation regions need to be covered by those ray tubes, which are then traced one by one to find their GO contributions at the location of the receiving antenna.

The basic ray-tracing procedure is described below.

1) Each ray of the ray tubes is traced to find an incident point (as shown in Fig. 2) where a ray propagates from a point $P_1(x_1, y_1, z_1)$ to an incident point $P_2(x_2, y_2, z_2)$ on an intercepting interface. The coordinates of the incident point P_2 can be determined from the following expression:

$$(x_2, y_2, z_2) = (x_1, y_1, z_1) + s\hat{s} \tag{1}$$

where $\hat{s}$ is the directional vector of the incident ray and s is the path length of the ray. For a flat interface defined with a normal unit vector $\hat{n} = (n_1, n_2, n_3)$ and a point $P_0 = (a, b, c)$ on the interface, the path length is given by

$$s = \frac{-(n_1x_1 + n_2y_1 + n_3z_1) + (an_1 + bn_2 + cn_3)}{s_1n_1 + s_2n_2 + s_3n_3} \tag{2}$$

which is obtained from the relation $\overrightarrow{P_0P_2} \cdot \hat{n} = 0$. For a finite-size interface, it is also necessary to check whether the incident point is within the boundary of the interface or not. All interfaces that may be illuminated by the ray tube should be tested to find the incident points and the incident point with the shortest path length from P_i is the true intercepting point. Except for the initial rays from the transmitting antenna, point P_1 is on an interface, too. Thus, for each interface that may start the ray tracing, based on the relative geometry of the structures, a list of the searching order over the other interfaces to find the incident point may be generated before starting the ray-tracing procedure to improve program efficiency.

2) When a ray tube incidents on an interface, a reflected and a transmitted ray tube is generated according to Snell's law and the local plane wave approximation. The reflection and transmission coefficients derived for a plane wave illuminating a flat interface of two lossless materials are employed [12]. However, complex dielectric constants are used instead of the lossless ones in the reflection/transmission coefficients and the propagation constants so that low lossy materials such as concrete and brick walls may be simulated. Multiple reflections/transmissions inside the materials are traced to properly determine the ray-tube penetrations through building structures.
3) A ray tube will be terminated if:
   1) it exits outdoor or leaves the simulated domain;
   2) it hits any edge of the structures (i.e., diffractions are neglected);
   3) the magnitude of the E-field is less than a threshold.

   For 3), the total length of the ray paths from the transmitting antenna to the present location is used to approximate the spreading factor of the E-field. A convergence test should be performed to set the proper threshold, which is defined as the percentage of the reference field strength at 1 m from the transmitting antenna. If both the reflected and transmitted rays are significant, one of the ray tubes is stored by pushing

it into a "stack," while the other one is continuously traced. The data set for each stored ray tube includes the directional vectors, positions, total path lengths, and E-field phasors (excluding the spreading factor) of the four rays. If both ray tubes are ended, a previously saved ray-tube data set is then popped from the stack and the ray-tracing procedure is started again. When the stack is empty, a new initial ray tube from the transmitting antenna is traced until finished. Multiple reflections and transmissions through walls, ceiling, stairs, floors, and other electrically large bodies can be simulated both in air and in the structures to properly model wave propagation and penetration in buildings.

4) When a ray tube enters the room containing the receiving antenna, as shown in Fig. 3, a test is then performed to determine whether or not this tube passes through the receiving point R. The ray tube entering the receiving room will be composed of four rays; otherwise, the ray tube has illuminated an edge of the structures and has been terminated in 3) already. The procedure of the test is described below.
   a) Find the four intercepting points O_i's of the ray-tube incident on a plane that is perpendicular to one of the four rays and contains the receiving point.
   b) Determine the four angles α_i's formed by O_i's and R with $0 \leq \alpha_i \leq \pi$.
   c) If the sum of the four angles α_i's is less than 2π, then the ray tube does not pass through R. However, 1.999π was actually employed instead of 2π in the comparison and double precisions were used to avoid possible numerical mistakes in determining the interception. The E-field vector phasors of the tubes passing the receiving point are superposed to obtain the E-field at this field point [11]. All the field points in the receiving room may be checked and evaluated during 4) to obtain the field distributions more efficiently.
5) From the geometrical optics, the E-field of the ray tube at the receiving point can be determined from the following equation:

$$\vec{E} = \vec{E}_0 \cdot \left\{\prod \overline{\overline{R}}_i\right\} \cdot \left\{\prod \overline{\overline{T}}_i\right\} \cdot \left\{\prod e^{-\gamma_i l_i}\right\} \cdot \mathrm{SF} \quad (3)$$

where $\vec{E}_0$ is the E-field at a reference point r_0, $\{\Pi^{\overline{R}_i}\}$ and $\{\Pi^{\overline{T}_i}\}$ are, respectively, the reflection and transmission coefficient dyads along the whole ray path, $\{\Pi^{e^{-\gamma_i l_i}}\}$ is the product of the propagation phase variations and exponential losses for this ray contribution starting from r_0, and SF is the spreading factor. From the conservation of energy flux in a ray tube [12], SF can be obtained by using

$$\mathrm{SF} = \sqrt{A_0}/\sqrt{A} \quad (4)$$

where A_0 and A are the cross-sectional areas of the ray tubes at the reference point r_0 and the field point r, respectively. The sum of the areas of the four triangles on the intercepting quadrilateral at the receiving point as shown in Fig. 3 may be evaluated to approximate the cross-sectional area A.

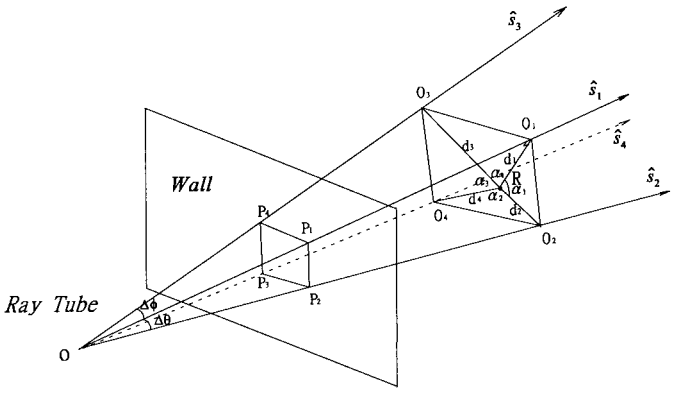

Fig. 3. A ray tube passing a receiving antenna at R.

Since both reflection and transmission ray tubes are traced at each interface and the spreading factor is determined from the cross-sectional area of the ray tube, this ray-tube tracing method can be applied to find the reflection and transmission contributions for rather complicated structures. In addition to flat slabs, shapes like wedges, rectangular cylinders, stairs, or curved blocks can be analyzed by using this approach to correctly evaluate the GO contributions including multiple reflections and transmissions.

III. Comparisons of the Ray-Tracing Method and the Moment Method

A ray-tracing program for both 2-D and 3-D structures has been developed according to the procedure described in the previous section. To simulate 2-D cases, the 3-D ray-tracing technique is modified slightly by fixing the center of each ray tube along the cross-sectional plane of the 2-D objects and using the arc-length instead of the area in (4) for determining the spreading factor. This section presents ray-tracing results for waves propagating in 2-D structures, and compares the results with those obtained from the MM. The solutions determined by the MM is numerically exact, as long as the segmentation of the objects is small enough. Due to the limitations of the computer memory and CPU time, the MM is usually applied for analyzing smaller objects in wavelengths. On the other hand, the ray-tracing method is a high-frequency approximation technique, which requires the dimensions of the objects be in the order of wavelengths or larger for accurate results. Therefore, the ray-tracing method is more suitable for modeling the indoor wave propagation for wireless communications. However, by choosing structures with dimensions around a few wavelengths, the MM can be used to check and verify the ray-tracing program.

A 2-D problem shown in Fig. 4 was simulated by using both the MM [8] and the ray-tracing method. An infinite unit electric-line source is located in the right-side room and the E-fields inside the other room are evaluated in the presence of a lossy half-space. Some results at the frequency of 450 MHz are given in Figs. 5 and 6 for lossless and lossy structures, respectively. The size of the structures is just a few

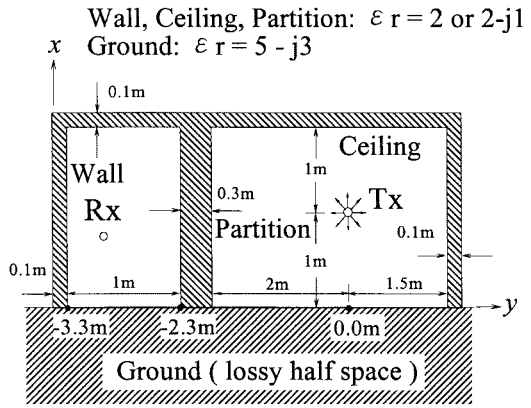

Fig. 4. An infinite line source radiates into a 2-D two-room structure.

wavelengths and can be accurately solved by the MM. Those dimensions are also large enough for the ray-tracing method. However, due to the GO approximations, some discontinuities exist in the ray-tracing results. Also, the locations and values of the peaks and valleys are slightly different between those two solutions. Higher order modes in MM (i.e., diffractions from edges and surface waves due to the lossy ground) will cause stronger resonance in the enclosed room and also remove the discontinuities. Nevertheless, the overall field variations obtained from those two methods are still quite similar. The good agreements between them verify most part of the ray-tracing program, since only the directions of the rays are restricted and 2-D spreading is used for solving the 2-D problems. Besides, the fields in the lossy case are about three times lower than those in the lossless case and, therefore, the good comparisons also suggest that the use of the complex dielectric constants in the lossless formula seem appropriate even for such a lossy material.

Fig. 7 shows a stair-shaped wall above a lossy ground illuminated by an infinite line source (Tx). The fields over the left side of the wall (Rx) were evaluated by using both the ray-tracing method and the MM. The results are given in Fig. 8, where the frequency is at 900 MHz and the complex dielectric constant of the wall $6.7-j1.2$ is to model reinforced concrete (RC) structures [9]. Since more discontinuities exist in the stair-shaped structures than those of the flat slabs in Fig. 4, the ray-tracing solutions in Fig. 8(a) indicate more abrupt field variations and larger errors due to the stronger higher order modes not included in the ray tracing. However, the ray-tracing results can still predict the overall level of the fields and locate the about positions of the peaks and valleys, especially at locations away from the wall. Since the rays may bounce between different sections of the stairs, multiple reflections inside the stair-shaped wall need to be traced and the variations of the spreading factor after reflections and transmissions should be properly evaluated, i.e., (4), to find the correct GO rays reflected from or transmitted through the stair-shaped wall.

IV. Comparisons of the Ray-Tracing Simulations and Field Measurements

This section presents field measurements and ray-tracing simulations for indoor radio-wave propagation and penetration.

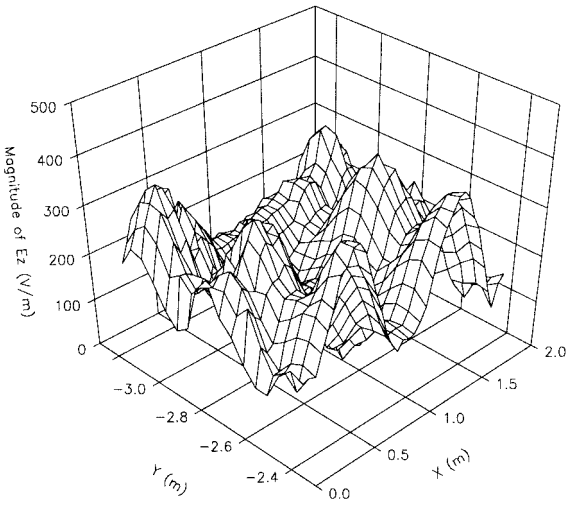

(a)

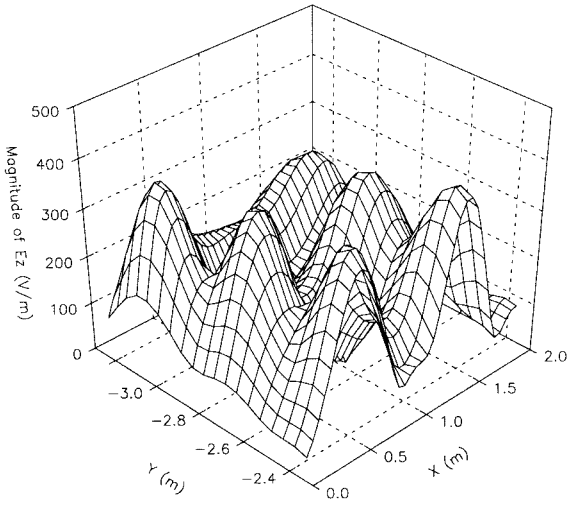

(b)

Fig. 5. E-field distributions at 450 MHz in the left-side room of Fig. 4 for lossless structures ($\varepsilon_r = 2$) determined from (a) the ray-tracing method and (b) the MM.

A vector network analyzer (VNA—HP8510C or HP8753B), an amplifier, and two dipole antennas were used to perform the measurements in a building at our university, as shown in Fig. 9. Results with the antennas located in a corridor, on different floors, and inside a staircase were tested and compared.

For the indoor measurements, a total of 801 S_{21} data points from 398 to 2798 MHz were measured at each field position with the dipole antennas being half wavelength long at 900 MHz. To remove outside noises/signals and improve the signal-to-noise (S/N) ratio, an average of 32 consecutive measurements had been taken at each frequency. The S_{21} of the VNA with the two antennas separated 1m apart and located 1.3 m above the floor near the center of the region between the elevator and the lower boundary of Fig. 9(a) were used as a reference. By dividing the measured S_{21} raw data of the field points with the reference at each frequency under the same measurement setup, the system parameters of the VNA and amplifier, cable losses, antenna factors, and mismatch effects

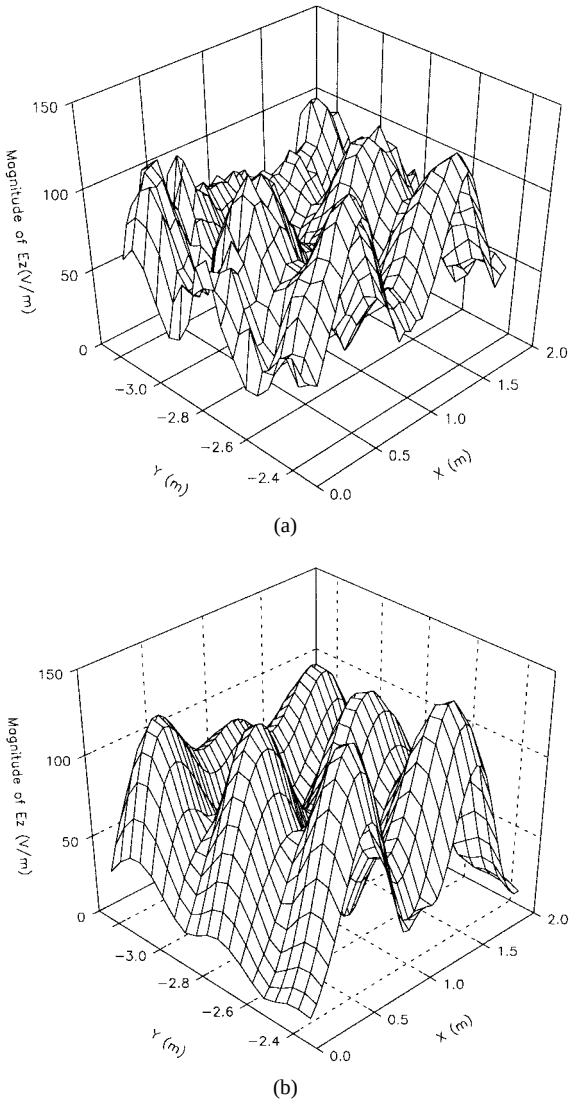

Fig. 6. E-field distributions at 450 MHz in the left-side room of Fig. 4 for lossy structures ($\varepsilon_r = 2 - j1$) determined from (a) the ray-tracing method and (b) the MM.

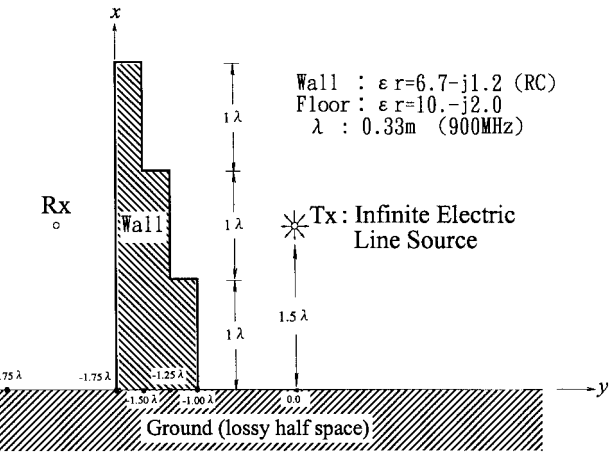

Fig. 7. An infinite line source radiates into a 2-D stair-shaped structure.

can be removed for a linear system. Fig. 10 plots an example of the open-site reference measurements, which indicate that those dipoles perform best at frequencies around 900 MHz and fair around 1800 MHz. Because the height of the ceiling from the floor is 3 m and the surrounding walls are at least 3 m away, the direct-path field of the reference dominates.

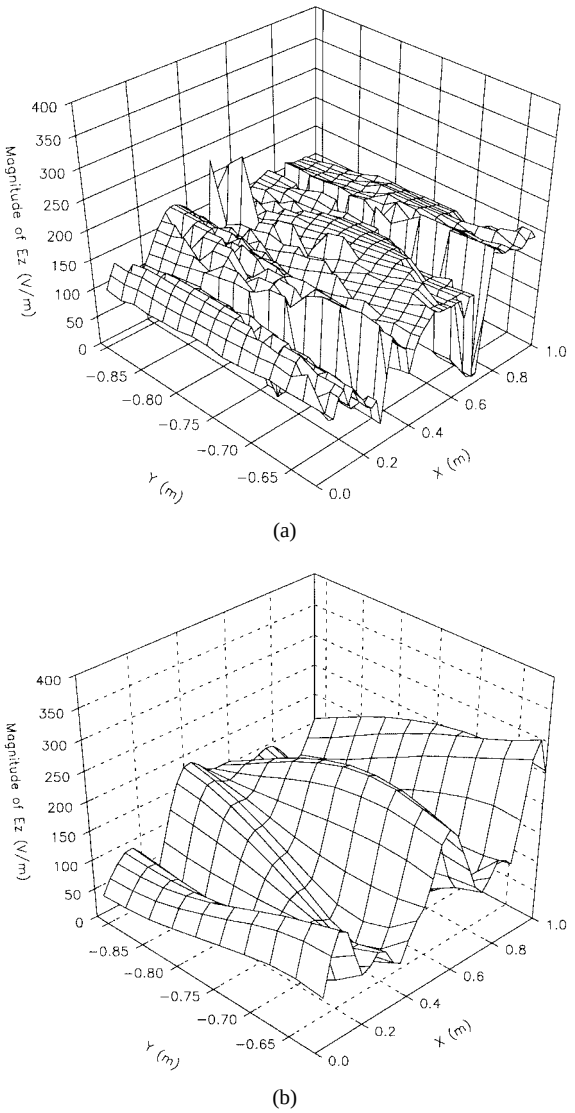

Fig. 8. E-field distributions at 900 MHz over the left side of the stair-shaped structure shown in Fig. 7 determined from (a) the ray-tracing method and (b) the MM.

For a plane wave incidence, the measured S_{21} of the VNA is proportional to the receiving antenna pattern in the reverse direction of the incident wave multiplied with the component of the incident E-field along the plane of the incident direction and the receiving dipole axis [13]. The ray-tracing program can be used to simulate the indoor wave propagation and penetration for determining the GO E-fields in the incident plane and then multiplying with the receiving antenna pattern factor to obtain the ray contributions to the receiving antenna. The phasor sum of all the significant ray contributions is evaluated at each field point. The setup for measuring the reference is also simulated by using the ray-tracing program. Then, by dividing the phasor sum at each field point with that evaluated for the reference, a ray-tracing calculated ratio can be obtained to compare with the measured S_{21} ratio. In the simulations, ideal sinusoidal current distributions and antenna patterns were assumed for the dipole antennas. Thus,

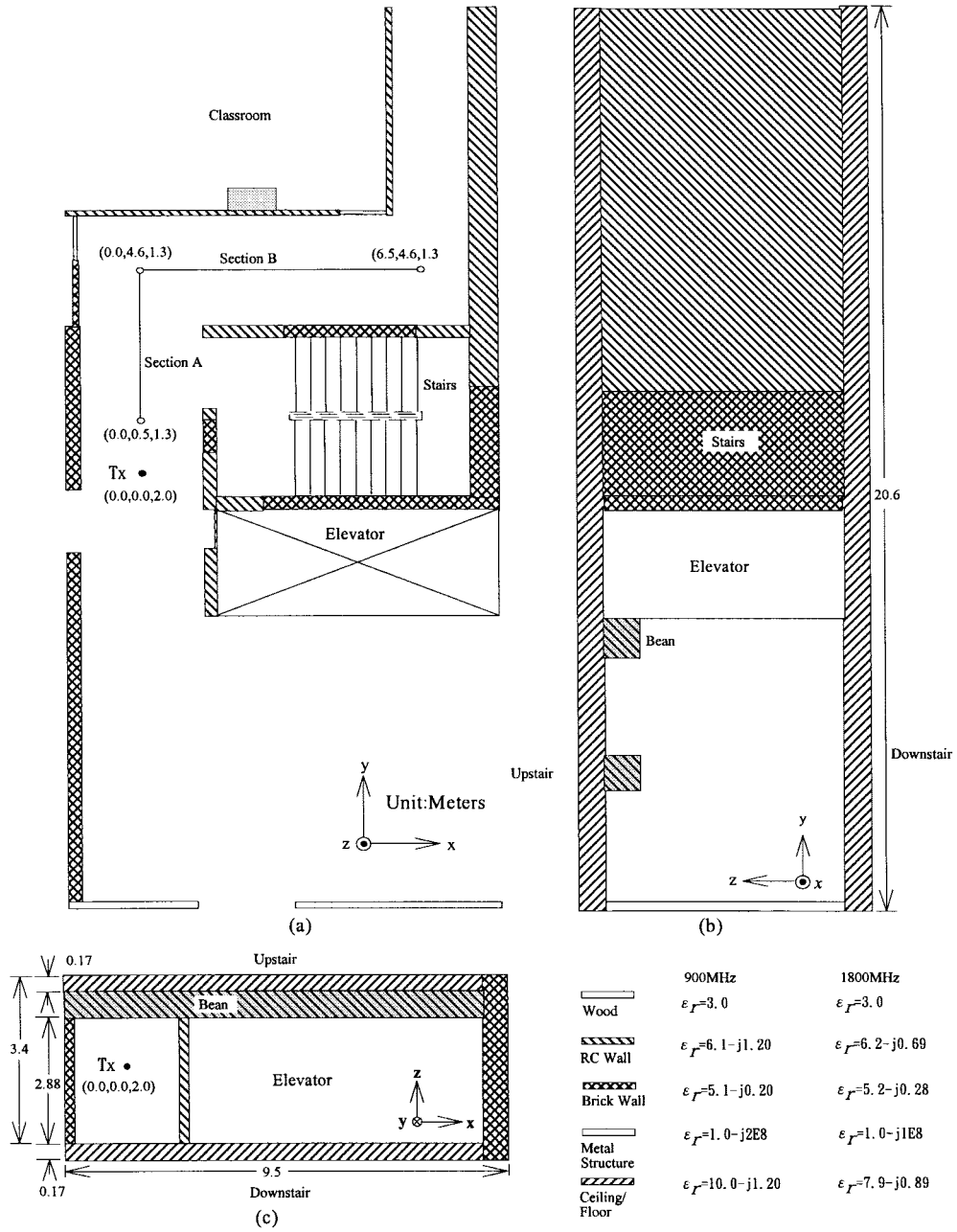

Fig. 9. A corridor in a building of National Taiwan University of Science and Technology (NTUST) for performing field measurements. (a) Top view. (b) Side view looking along the x direction. (c) Side view looking along the y direction.

for a z-polarized dipole of length $2h$ located at the origin, the following two equations [13]

$$\vec{I}(z) = \hat{a}_z I_m \sin\beta(h - |z|) \quad \text{(A)} \tag{5}$$

and

$$\vec{E}(r,\theta) = \hat{a}_\theta \frac{j60I_m}{r} e^{-j\beta r} \frac{\cos(\beta h\cos\theta) - \cos\beta h}{\sin\theta} \quad (\text{V/m}) \tag{6}$$

were used to approximate the current and the radiating E-field in free space. Also, the building structures were modeled with homogeneous slabs and blocks having effective complex dielectric constants obtained from a free-space method using transmission measurements at normal incidence [9]. Thus, only the major effects of the structures were considered.

For the case in a corridor, the transmitting antenna was fixed at a location, while the receiving antenna was moved along an L-shaped path, i.e., Sections A and B in Fig. 9 with both the dipoles polarized vertically (the z direction). As shown in Fig. 9, some of the walls are composed of the RC and brick structures, which were indicated in the blueprint of the corridor and also verified by the material property measurements. The correct modeling of the walls is important since the path–loss difference between the RC and brick walls is significant. Figs. 11 and 12 compare the measured and simulated ratios of the E-fields along the L-shaped corridor for different antenna heights and frequencies. Also, ray-tracing results with three different $\Delta\theta$'s are presented in Fig. 12 for the 900-MHz case with different transmitting and receiving antenna heights to

TABLE I
CPU TIME AND ERRORS FOR THE CASE GIVEN IN FIG. 12(a) WITH A 5% THRESHOLD

$\Delta\theta$ (Degrees)	CPU Time on Pentium-166 (H:M:S)	Average Errors (Compared with Measurements) (dB)	Standard Deviations (Compared with Measurements) (dB)	Average Errors (Compared with $\Delta\theta=1^\circ$ Simulations) (dB)	Standard Deviations (Compared with $\Delta\theta=1^\circ$ Simulations) (dB)
1.0	57:16	-0.429	3.98	0	0
1.5	24:34	-0.426	3.98	-0.084	1.03
2.0	13:26	-0.316	3.70	-0.004	0.97
2.5	8:22	-0.250	3.53	0.103	1.35
3.0	5:39	-0.486	3.75	-0.089	2.92

TABLE II
CPU TIME AND ERRORS FOR THE CASE GIVEN IN FIG. 12(b) WITH A 0.5% THRESHOLD

$\Delta\theta$ (Degrees)	CPU Time on Pentium-166 (H:M:S)	Average Errors (Compared with Measurements) (dB)	Standard Deviations (Compared with Measurements) (dB)	Average Errors (Compared with $\Delta\theta=1^\circ$ Simulations) (dB)	Standard Deviations (Compared with $\Delta\theta=1^\circ$ Simulations) (dB)
1.0	1:50:26	-0.878	5.10	0	0
1.5	45:00	-0.760	5.22	0.118	2.50
2.0	23:42	-0.874	5.17	0.004	2.50
2.5	14:10	-0.699	5.06	0.179	2.82
3.0	9:22	-1.458	5.85	-0.580	3.51

show the convergence of the solutions. In addition, Tables I and II compare the amounts of CPU time on Pentium 166 needed to perform the 900-MHz simulations and also list the averages and standard deviations over the differences between the simulations and measurements in decibels for five different $\Delta\theta$'s. The average values of the measured data in decibels are only slightly lower than those obtained from ray-tracing simulations. However, the standard deviations are about 4 dB in Fig. 12(a) and 5 dB in Fig. 12(b). The value of $\Delta\theta(\Delta\phi \cong \Delta\theta/\sin\theta)$ significantly affects the required running time and should be small enough to obtain convergent results. A $\Delta\theta$ of 3° is already good enough for this case. For all other cases measured at the NTUST shown in this paper, only the simulated data with $\Delta\theta = 1^\circ$ are presented.

The simulated results shown in Figs. 11 and 12 follow the trend of the measurements. Most of the peaks and valleys of the measurements also coincide well with those of the simulations, although the scattering from following objects were not included in the simulations: roughness and inhomogeneity of the walls, edges of the structures, power cables in plastic pipes hung on the ceiling, electrical wires inside the structures, and other details. For the waves propagating in the L-shaped corridor, the reflections from the ceiling of the upstairs and the floor of the downstairs are negligible due to the higher round-trip attenuation through the ceiling and floor. Actually, a 2-D approach by considering only the rays propagating in the horizontal and vertical planes on the same floor may be applied to obtain results close to those from the 3-D ray-tracing program much more efficiently [7].

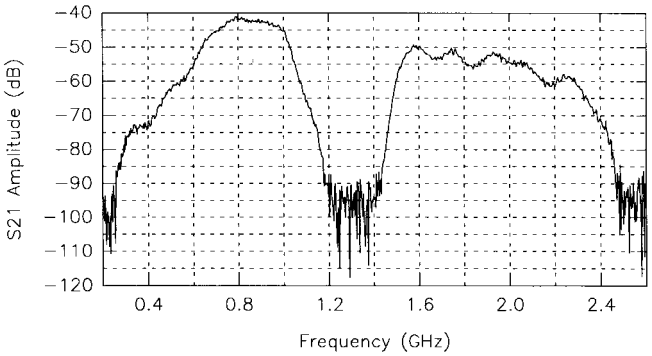

Fig. 10. An example of the open-site measurements. The dipole antennas are a half-wavelength long at 900 MHz.

Fig. 13 plots the geometry of the setup for the dipole antennas on different floors and also the measured and simulated S_{21} ratios at frequencies of 900 and 1800 MHz with both the dipoles polarized horizontally along the y direction. The receiving antenna (Rx) was moved along a straight path directly above the transmitting antenna (Tx). As shown in Fig. 13(b) and (c), the simulations and measurements are close in part of the path, but may be more than 5 dB different at locations away from Tx. The measurements of the dielectric constants of the ceiling used in the simulations were taken at the location of Tx under normal incidence. Therefore, the differences of the results are most likely due to the inhomogeneity of the ceiling, which are modeled as homogeneous flat slabs in the simulations.

The geometry of the measurement site for waves propagating in a staircase is plotted in Fig. 14, where Tx is located on the third floor and Rx is moved along a cross path (Sections A and B) on the stage between the second and third floors. Results of the field measurements and ray-tracing simulations are shown in Fig. 15 for frequencies at 900 and 1800 MHz. The dielectric constant of the stair structure used in the simulations was assumed to be that of the RC wall since the free-space method for measuring the dielectric constant is not applicable for the stairs. Better agreements are achieved at the higher frequency. The differences between the measurements and simulations may be due to the following reasons.

1) The diffractions from the edges of the stair structures are not included in the simulations.
2) The dimensions of each stair step are less than a wavelength at 900 MHz. Since the ray-tracing method is a high-frequency approximation technique, larger error is expected at the lower frequency for smaller dimensions.
3) The effective complex dielectric constants used for the stairs and side walls are only a rough approximation for the composite building structures. Also, since the building structures are modeled as homogeneous blocks, the scattering due to the inhomogeneous composite materials can cause significant modeling errors in phases and magnitudes.

Nevertheless, the agreements between the measurements and simulations for the complicated stair geometry are still good.

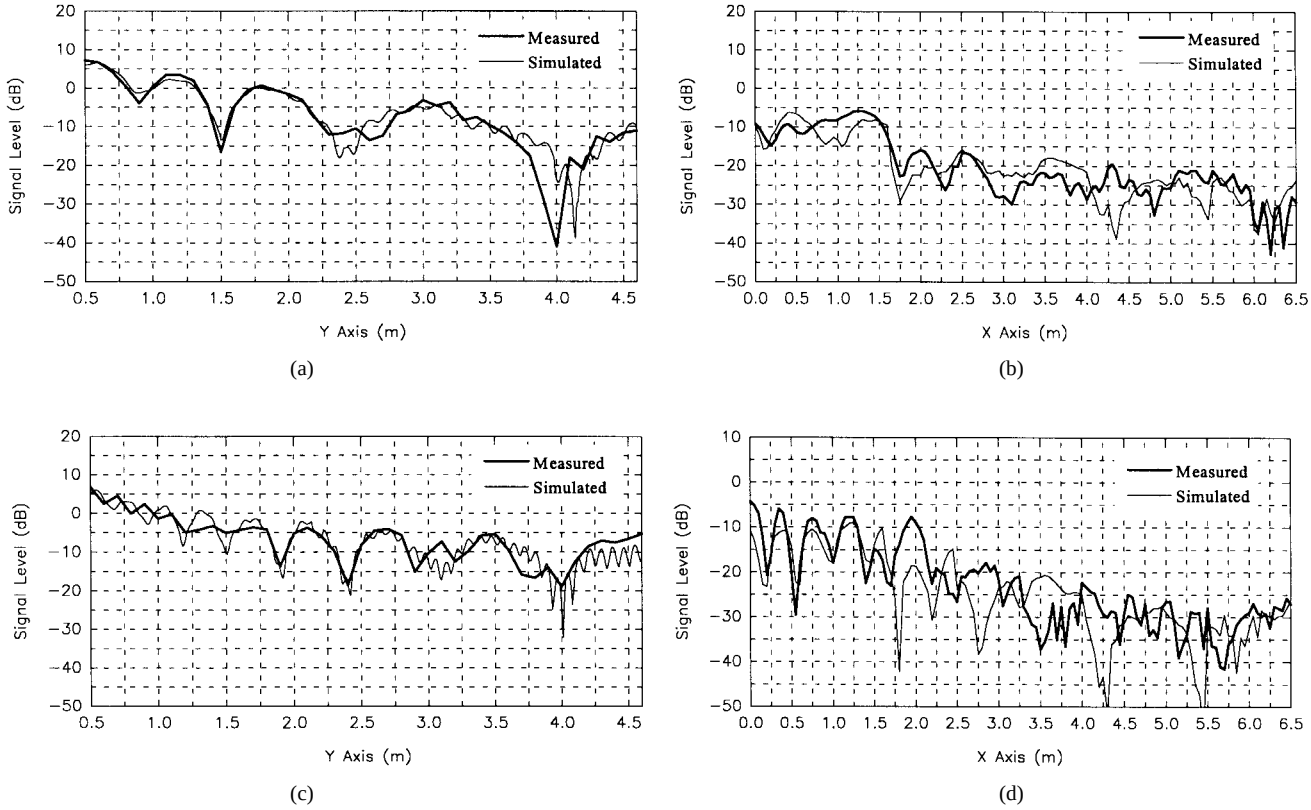

Fig. 11. Comparisons of the field measurements and ray-tracing simulations along the corridor for both the antennas located at the same height (1.3 m) and polarized vertically. (a) Section A, 900 MHz. (b) Section B, 900 MHz. (c) Section A, 1800 MHz. (d) Section B, 1800 MHz.

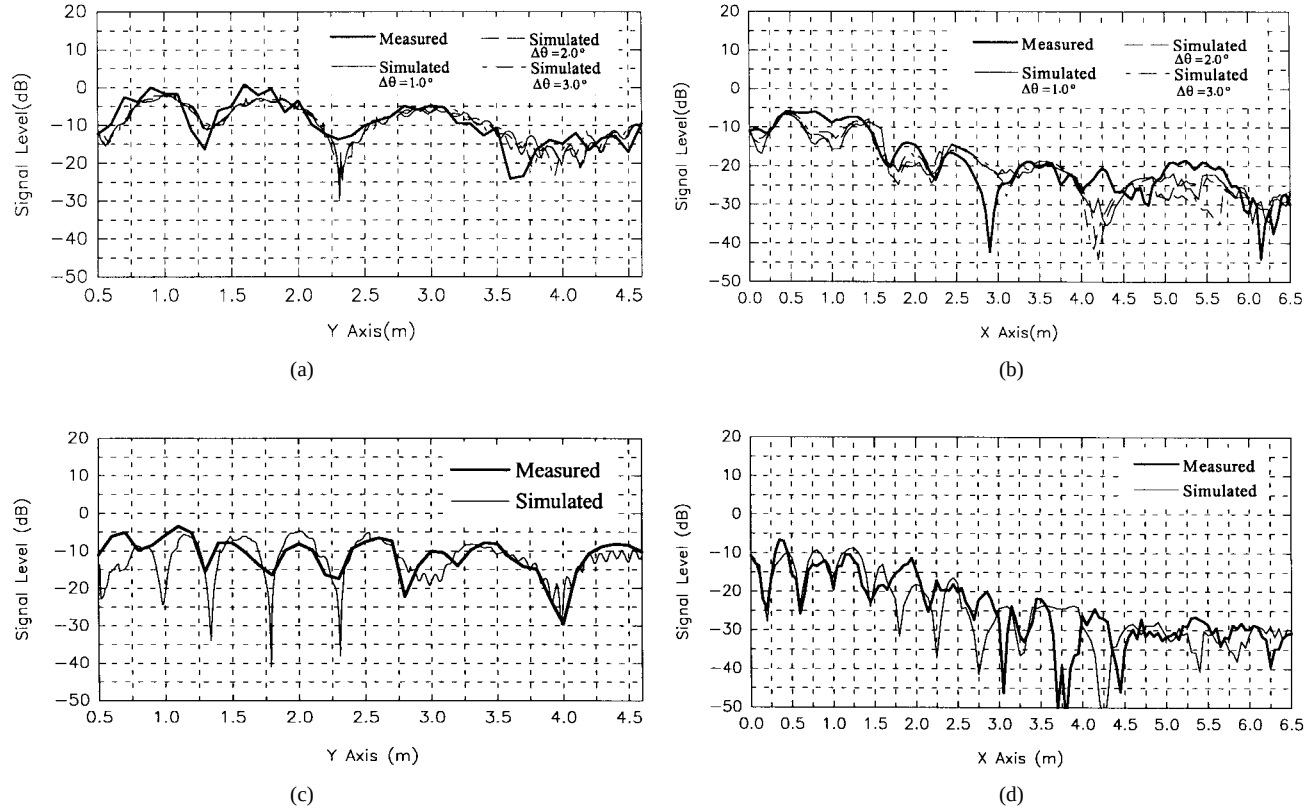

Fig. 12. Comparisons of the field measurements and ray-tracing simulations along the corridor for the antennas located at different heights (Tx: 1.96 m; Rx: 1.3 m) and polarized vertically. (a) Section A, 900 MHz. (b) Section B, 900 MHz. (c) Section A, 1800 MHz. (d) Section B, 1800 MHz.

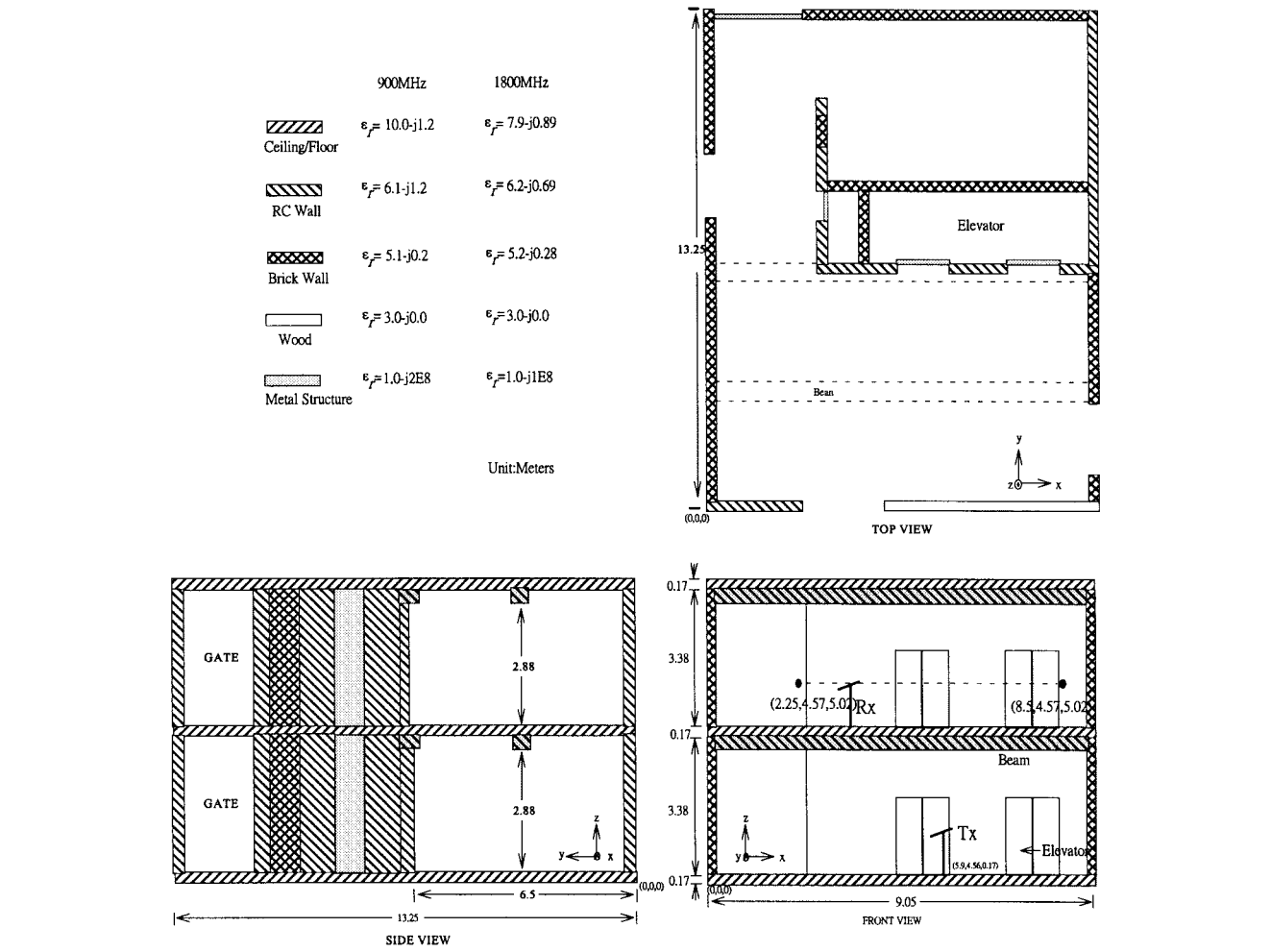

Fig. 13. Comparisons of the field measurements and ray-tracing simulations for the antennas located at different floors and polarized horizontally along the y direction. (a) The measurement site. (b) Results at 900 MHz. (c) Results at 1800 MHz.

Table III lists the amounts of CPU time on Pentium 166 spent in the ray-tracing simulations for those measurements performed at the NTUST. The 3-D ray-tracing program by using ray tubes with $\Delta\theta = 1°$ and $\Delta\phi \cong \Delta\theta/\sin\theta$ are employed in those calculations, where the ray tubes are traced one by one. Considerable improvement of the running efficiency may be achieved by first finding the angular regions of ray tubes that may enter a receiving boundary including all the Rx locations. Some test rays equally covering the whole radiation sphere from Tx can be traced to determine those angular regions. Then, detailed tracing for all the tubes in only those regions is performed.

Fig. 16 demonstrates a comparison of the measurements and simulations for waves penetrating through an exterior wall with windows. The measured data are taken from [10], where a room of 16 m $\times$ 6 m is illuminated by a Tx at a distance of 888 m away from the wall and incident at an angle of 3° off the normal of the wall surface and the locations of the

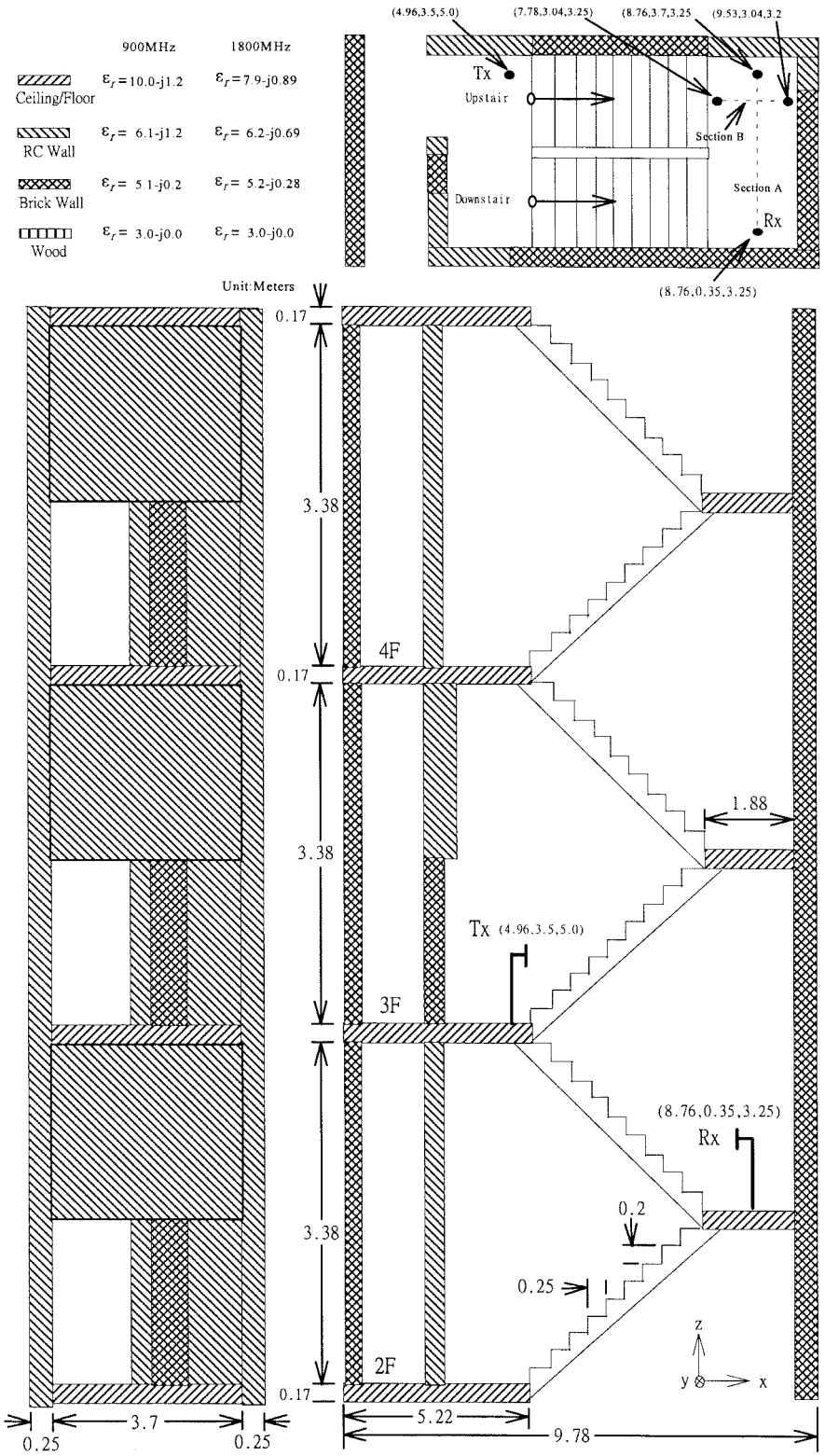

Fig. 14. A staircase in a building of the NTUST for performing field measurements.

Rx were only 1 m behind the inner surface of the exterior wall. A vertically polarized Yagi array of 23 elements and a standard dipole antenna were used as the Tx and Rx in those measurements. The geometry of the room modeled in our ray-tracing simulations is plotted in Fig. 16(a), together with the material properties assumed and a vertically polarized half-wave dipole at 1290 MHz is transmitting instead of the Yagi array for simulating this far-zone illumination. The E-field strength in dBmV/m for the half-wave dipole with 20-dB ampere maximum current is plotted in Fig. 16(b) compared with the results presented in [10] (the dimension of the field strength of the measured data is not clear and the antenna

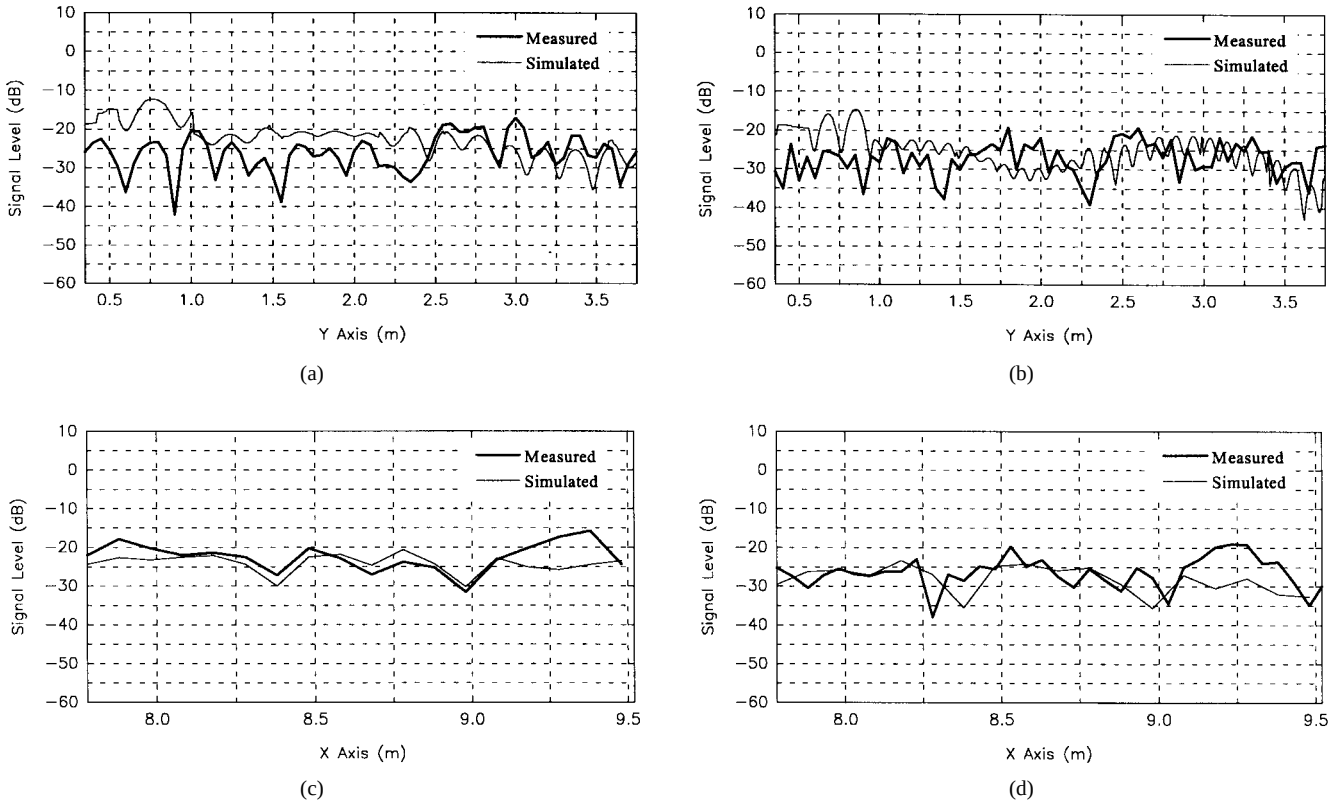

Fig. 15. Comparisons of the field measurements and ray-tracing simulations for the staircase of Fig. 14. The antennas are polarized vertically. (a) Section A, 900 MHz. (b) Section A, 1800 MHz. (c) Section B, 900 MHz. (d) Section B, 1800 MHz.

TABLE III
COMPARISONS OF CPU TIME REQUIRED TO RUN THE RAY-TRACING SIMULATIONS WITH $\Delta\theta = 1°$ FOR THE CASES TESTED IN THE BUILDING OF NTUST

Cases	Threshold (%)	CPU Time on Pentium-166 (H:M:S)	Cases	Threshold (%)	CPU Time on Pentium-166 (H:M:S)
Fig.11(a)	5.0	1:05:20	Fig.11(b)	0.5	1:53:05
Fig.11(c)	5.0	1:05:06	Fig.11(d)	0.5	1:44:07
Fig.12(a)	5.0	57:17	Fig.12(b)	0.5	1:50:26
Fig.12(c)	5.0	1:20:32	Fig.12(d)	0.5	1:41:55
Fig.13(b)	1.0	3:11:23	Fig.13(c)	1.0	2:03:44
Fig.15(a)	1.0	4:54:53	Fig.15(b)	1.0	3:09:59
Fig.15(c)	1.0	5:29:33	Fig.15(d)	1.0	4:02:48

factors are unknown). The effects of the window frames are not included in the simulations. From this comparison, some observations are given below.

1) Since the path of the Rx locations is nearly normal to the incident rays and parallel to the exterior and interior walls, the GO contributions should vary smooth along the path, as is indicated in the ray-tracing results.
2) The ripples with about a one wavelength separation occur in the measurements and the trend of the field strength is slowly varied too. Those phenomena may be due to the scattering effects of the array of the long metal window frames parallel to the vertically polarized incident fields. Also, the array of the frames are close to the Rx and parallel to the receiving path. Thus, the scattered fields from those frames can be strong and result in fast fading and field variations.
3) The concrete posts of the exterior walls attenuate the fields significantly as shown both in the measured and simulated data.

V. CONCLUSIONS

A ray-tracing program has been developed for modeling indoor wave propagation and penetration. Multiple reflections and transmissions of ray tubes inside and among walls, ceilings/floors, and other building structures are traced to determine the GO contributions. Each ray tube is composed of four rays defining by $\Delta\theta$ and $\Delta\phi$ in a local spherical coordinate system centered at the transmitting antenna, and the solid angles of the initial ray tubes are kept approximately the same. To accurately model the spreading of the tubes reflected or transmitted through complex structures, the ray tubes are traced and the cross-sectional areas of the tubes are evaluated at the receiving locations to determine the spreading factors based on the conservation of energy flux in a ray tube.

Ray-tracing solutions for a 2-D two-room structure and also a 2-D stair-shaped wall above a lossy ground have been compared with those determined from the MM. Good agreements have been obtained. Also, field measurements to find the field distributions in a corridor, on different floors, and inside a staircase have been performed by using a vector network analyzer, an amplifier, and two dipole antennas. Line-of-sight measurements in a large empty region with the

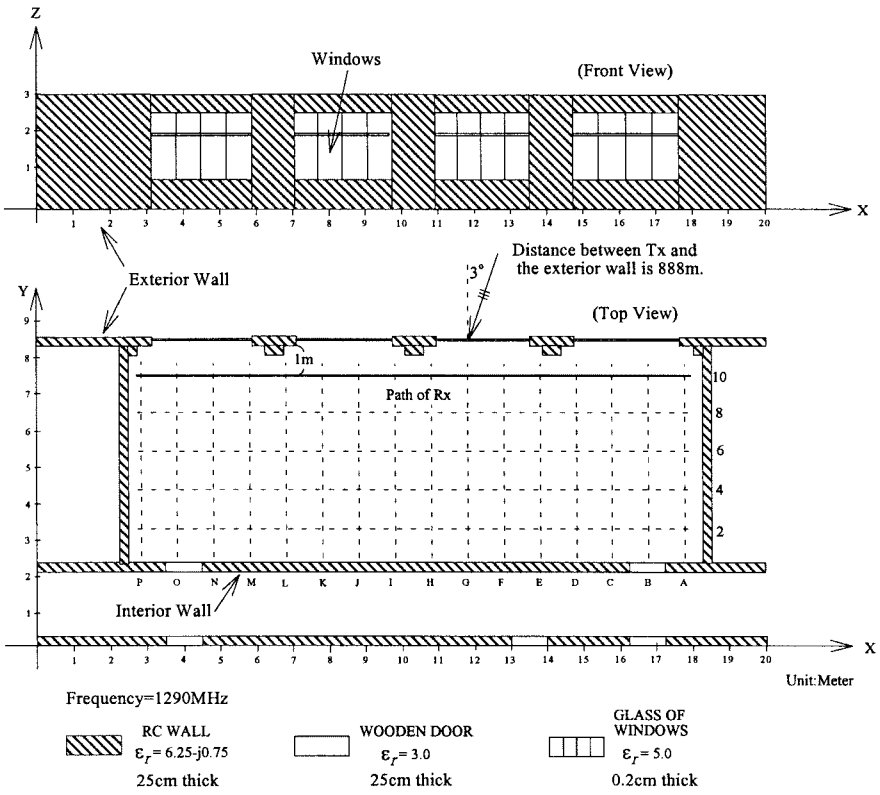

(a)

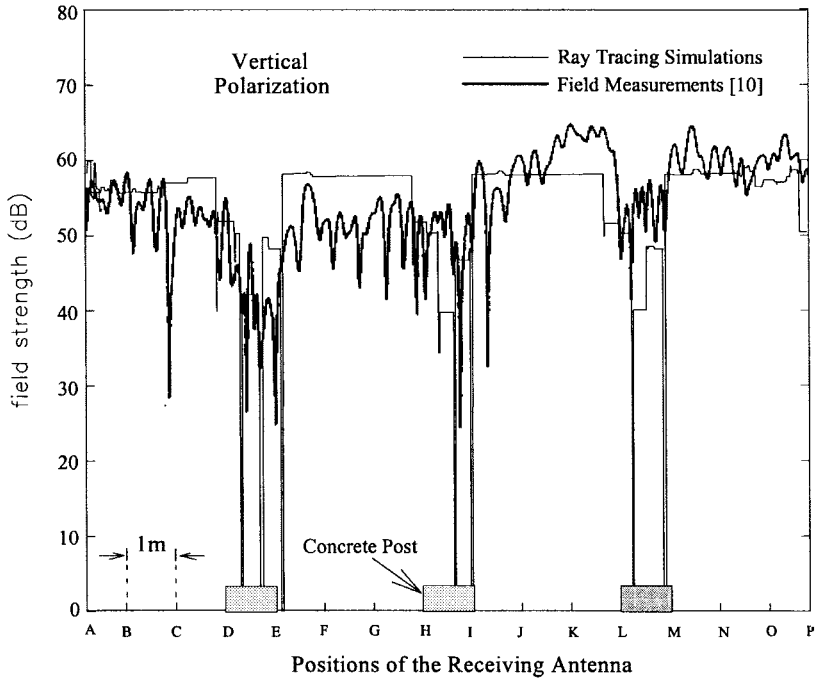

(b)

Fig. 16. Penetrations of waves at 1290 MHz through an exterior wall with metal-framed windows for a case reported in [10]. (a) Geometry and material properties used in our ray-tracing simulations. (b) Comparisons of the ray-tracing simulations and the field measurements given in [10].

transmitting and receiving antennas separated by 1 m were employed as the reference of the field measurements. Then, the ray-tracing program has been applied to evaluate the fields at 900 and 1800 MHz in the buildings for comparisons with the measurements. The complex dielectric constants of the RC walls, brick walls, and floors determined from a free-space method were employed in the simulations. The simulated solutions mostly follow the trend of the measured results. Furthermore, measured data at a frequency of 1290 MHz from [10] for waves penetrating an exterior wall with several

metal-framed windows are employed to examine the ray-tracing solutions at receiving locations close to the windows. Scattering from the metal frames seems important for this case.

This ray-tube tracing method may be applied to model the wave propagation in and penetration through arbitrary shapes of electrically large building structures that do not excite significant diffracted fields to the receiving locations. Results obtained from this ray-tracing program can be employed to study the channel characteristics of the indoor wireless communications.

ACKNOWLEDGMENT

The authors would like to thank S.-S. Chuang and W.-K. Liang for performing the field measurements.

REFERENCES

[1] W. Honcharenko, H. L. Dailing, and J. Dailing, "Mechanisms governing propagation between different floors in buildings," *IEEE Trans. Antennas Propagat.*, vol. 41, pp. 787–790, June 1993.
[2] H. L. Bertoni, W. Honcharenko, L. R. Maciel, and H. H. Xia, "UHF propagation prediction for wireless personal communications," *Proc. IEEE*, vol. 82, pp. 1333–1359, Sept. 1994.
[3] S. Y. Seidel and T. S. Rappaport, "Site-specific propagation prediction for wireless in-building personal communication system design," *IEEE Trans. Veh. Technol.*, vol. 43, pp. 879–891, Nov. 1994.
[4] U. Dersch and E. Zollinger, "Propagation mechanisms in microcell and indoor environments," *IEEE Trans. Veh. Technol.*, vol. 43, pp. 1058–1066, Nov. 1994.
[5] S.-H. Chen and S.-K. Jeng, "An SBR/image approach for indoor radio propagation in a corridor," *IEICE Trans. Electron.*, vol. E78C, no. 8, pp. 1058–1062, Aug. 1995.
[6] P. T. Davis and C. R. Mcguffin, *Wireless Local Area Networks: Technology, Issues, and Strategies*. New York: McGraw-Hill, 1995.
[7] K. Pahlavan and A. H. Levesque, *Wireless Information Networks*. New York: Wiley, 1995.
[8] C.-F. Yang and T.-S. Wang, "A moment method solution for TMz and TEz waves illuminating two-dimensional objects above a lossy half space," *IEEE Trans. Electromagn. Compat.*, vol. 38, pp. 433–440, Aug. 1996.
[9] C.-F. Yang, C.-J. Ko, and B.-C. Wu, "A free space approach for extracting the equivalent dielectric constants of the walls in buildings," in *IEEE AP-S Int. Symp. URSI Radio Sci. Meet.*, Baltimore, MD, July 1996, pp. 1036–1039.
[10] J. Horikoshi, K. Tanaka, and T. Morinaga, "1.2 GHz band wave propagation measurements in concrete building for indoor radio communications," *IEEE Trans. Veh. Technol.*, vol. VT-35, pp. 146–151, Nov. 1986.
[11] H. Kim and H. Ling, "Electromagnetic scattering from an inhomogeneous object by ray tracing," *IEEE Trans. Antennas Propagat.*, vol. 40, pp. 517–525, May 1992.
[12] C. A. Balanis, *Advanced Engineering Electromagnetics*. New York: Wiley, 1989.
[13] W. L. Stutzman and G. A. Thiele, *Antenna Theory and Design*. New York: Wiley, 1981.

Chang-Fa Yang (S'86–M'92) was born in Taipei, Taiwan, R.O.C., on October 14, 1960. He received the B.S. degree from the National Taiwan University, Taipei, in 1983, and the M.S. and Ph.D. degrees from The Ohio State University, Columbus, in 1988 and 1992, respectively, all in electrical engineering.

From 1986 to 1992, he was a Graduate Research Aassociate with the ElectroScience Laboratory, Columbus, OH. In February 1992 he joined the faculty of the National Taiwan University of Science and Technology, where he is now an Associate Professor. His research interests include numerical methods, wireless communications, and electromagnetic interferences at power and microwave frequencies.

Boau-Cheng Wu was born in Kaohsiung, Taiwan, R.O.C., on June 5, 1971. He received the B.S. and M.S. degrees in electrical engineering from the National Taiwan University of Science and Technology, Taipei, in 1995 and 1998, respectively.

His research interests include wireless communications and automatic controls.

Chuen-Jyi Ko was born in Changhua, Taiwan, R.O.C., on November 18, 1964. He received the B.S. and M.S. degrees in electrical engineering from the National Taiwan University of Science and Technology, Taipei, in 1990 and 1996, respectively.

He is currently with the Chunghwa Telecommunication Company, Taipei. His research interests are in wireless communications.